

Simulating Proton Transport through a Simplified Model for Trans-Membrane Proteins

Lynsey M. S. Shepherd and Carole A. Morrison*

School of Chemistry and EaSTCHEM Research School, The University of Edinburgh, King's Buildings, West Mains Road, Edinburgh, EH9 3JJ, U.K.

Received: October 27, 2009; Revised Manuscript Received: April 19, 2010

Ab initio MD simulations on a polyglycine helix and water-wire expressed under periodic boundary conditions have created a channel that supports proton transfer up to distances of 10.5 Å. The effect of varying the density of water molecules in the channel has been investigated. A range of cationic states are identified with widely varying lifetimes. The mechanism of proton transport in this model shares some features with the simulations reported for bulk water, with, e.g., the hydrogen bond distance shortening in the time period leading up to successful proton transfer. However, there are also some important differences such as the observation of a heightened number of proton rattling events. We also observe that the helix plays an important role in directing the behavior of the water wire: the most active proton transport regions of the water-wire are found in areas where the helix is most tightly coiled. Finally, we report on the effects of different DFT functionals to model a water-wire and on the importance of including dispersion corrections to stabilize the α-helical structure.

I. Introduction

Proton transport (PT) across cell membranes is of fundamental importance in chemical biology, giving rise to many basic functions including bioenergetics, cell signaling, and pH regulation.^{1–3} While PT is known to occur via transient water molecules across the cell membrane itself, it is more often the case that the mechanism involves proteins that span the membrane surface and act as proton-specific ion channels. Evidence for the relay of H⁺ by buried water molecules (“water wires”) mediated by the side chains of α-helices has been substantiated in several channel and signaling trans-membrane proteins. Specific systems include the ion channel protein bacteriorhodopsin,⁴ the M2 channel of the influenza A virus,⁵ the MotA–MotB protein component of the flagella that drive *Escherichia coli*,⁶ and the aquaporins.⁷ The coding for membrane-bound proteins constitutes 25–30% of all genes, and they are implicated in many diseases such as diabetes and Parkinson’s. Consequently, they are the subject of major drug target studies (in fact, the drug targets for all neurological diseases are membrane-bound proteins). Their importance was further recognized in 2003 when the Nobel Prize for Chemistry was awarded to Agre and MacKinnon for their discoveries concerning channels in cell membranes.

Finding direct experimental evidence for PT is extremely challenging work. The protons are thought to be carried by a chain of water molecules, but this level of detail lies beyond the current limit for experiment. Electrophysiology experiments can provide a qualitative picture of the conduction properties of a channel by voltage measurement, but it is difficult to obtain a clear picture of what is happening. Crystal structures can also provide insight, but it too is limited. To date, the most complete atomistic models available for a trans-membrane protein are those for bacteriorhodopsin and its analogue, bovine rhodopsin, both of which are applied via homology modeling as general models for membrane-bound drug target proteins.^{8–10} The bacteriorhodopsin structure was obtained from high-resolution

electron microscopy data supplemented with X-ray diffraction data of 1.55 Å resolution.¹¹ While this is currently state-of-the-art, it is still possible to miss-assign amino acid residues, and hydrogen atom positions are far beyond reach. In addition, concerns exist as to whether the protein is captured in its active or passive form. All of these issues have critical implications in understanding how the protein functions from an atomistic level.

When experimental methods yield only partial results, it is the role of theory to complete the story. The accurate modeling of PT events also presents its own challenges, however, as the mechanism involves bond making/breaking events, which requires that a high level of computational modeling such as quantum mechanics (QM) is employed. In addition, hydrogen atoms may quantum tunnel, and along with zero-point energy affects this may radically alter the reaction landscape. To further compound these problems, the proton hop step is a borderline rare event, meaning that some computational effort will be “wasted” on the uninteresting wait time between events, resulting in obvious problems with statistical sampling. As with all simulations in chemical biology, a balance must be struck between a realistic (i.e., atom-rich) model that can only be supported by a low-to-medium level of computational accuracy [such as classical molecular modeling (MM) and its extensions MS-EVB^{12–14} and QM/MM^{15,16}] and a simplified, less realistic, atom-light model that can be subjected to the higher-level quantum mechanical-based methods. Examples of the first all-atom approach are plentiful in the literature, with most attention understandably focused on small, structurally well-defined TMPs such as bacteriorhodopsin,^{17–19} the M2 channel of the Influenza A virus,^{20,21} and cytochrome C oxidase.^{22–25} Another example is the use of the synthetic leucine-serine channel (LS2)²⁶ to study PT, although this model is still too large to allow for full QM methods.^{27,28} We stress that if the PT mechanism is suspected to involve a water-wire system then it is important that the simulation takes this into account, rather than opting for the simpler unprotonated water chain system, as their behaviors can be markedly different.²⁹

* Corresponding author. E-mail: c.morrison@ed.ac.uk.

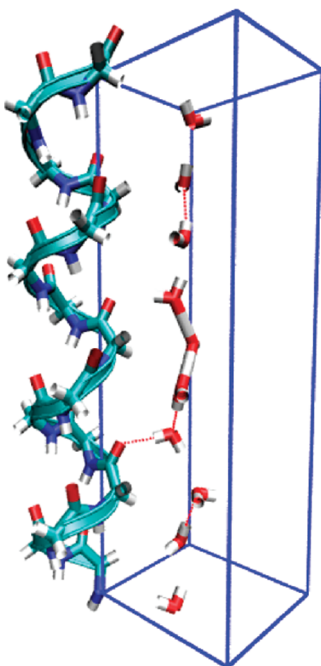


Figure 1. Ten-molecule water-wire simulation model.

Simplified models have in the past provided valuable insight into the process of PT through membrane-bound proteins and offer the considerable benefit that their simplicity allows generic principles to be obtained. Both restraining potentials in vacuo^{30,31} and carbon nanotubes^{32–35} have been successfully employed to model a nonpolar pore in which water molecules are confined. The resulting PT steps observed are consistent with the general idea behind the Grotthuss mechanism,³⁶ i.e., the proton “hops” along a hydrogen-bonded chain of water molecules. The critical feature of this mechanism is that the identity of the transferring proton changes, enabling faster transport than conventional diffusion of the H_3O^+ species. The hydrogen bond donor–acceptor distance plays a critical role, as shortening this distance (that is, forming a Zundel or $[\text{H}_5\text{O}_2]^+$ species) reduces the barrier height in the double well potential, thus facilitating the proton “hop” step. A model with greater chemical relevancy is the α -helical polyglycine analogue of the gramicidin A channel with a water-wire inserted into the internal cavity of the helix.³⁷ This model has been studied using QM simulations and found to support PT. In fact this model-concept is very similar to the work presented here, but we take a polyglycine α -helix expressed under periodic boundary conditions (PBCs) as our base model, which mimics a tertiary structure much more commonly found in TMPs.

To take a specific example of an α -helical domain, the simplest and most common structural motif consists of a bundle of four almost parallel helices.³⁸ We can mimic this with a model constructed from an orthorhombic box with lattice vectors $a = c$; the α -helices and water chain will lie along the b -axis (see Figure 1). PBCs can then be applied to build an infinite array of continuous channels, removing the requirement to build in a water reservoir at the entrance and exit sites of the channel (see Figure 2). The interhelical distance (and thus the diameter of the central cavity) is varied directly by the a, c lattice vectors. Due to the demands of the PBCs, the length of the b -vector relates to a single α -helical pitch, which also happily corresponds to the typical depth of a trans-membrane protein. By making use of PBCs in this way, we can therefore utilize just one α -helix and one water environment to build our channel

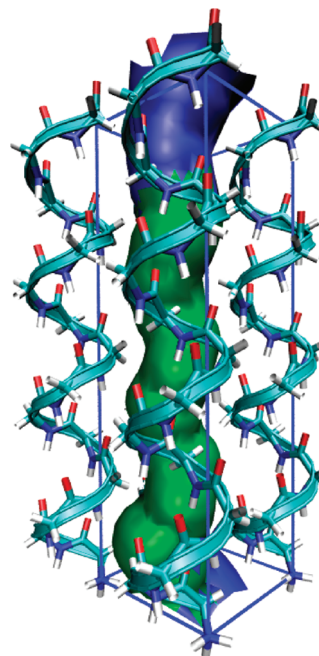


Figure 2. Simulation model showing the internal cavity of the simulation cell, into which eight, ten, or twelve water molecules plus an extra proton are placed. The color scheme is an indicator of pore radius, with green denoting an intermediate range of 1.5–2.3 Å and blue a wider range of $r > 2.3$ Å (note the wider ends are an artifact of the cavity being calculated based on one simulation cell, rather than an infinite channel).

environment. The downside is, of course, that we must accept that the infinite arrays are composed of identical copies of these building blocks, but the tremendous upside is that this model-system comprises less than 150 atoms, meaning that full quantum mechanical simulations are a realistic option, thus allowing the bond making and breaking steps to be treated appropriately and molecular dynamics (MD) simulations of the order of tens of picoseconds to be realistically harvested, thereby minimizing the problems associated with rare-event sampling. In fact, to the best of our knowledge, these simulations are the first report of an α -helical channel/water-wire system performed entirely at the quantum mechanical level.

A potential criticism can, however, be levied at ab initio MD calculations when applied to study PT reactions. The many-electron Hamiltonian is approximated by density functional theory (DFT), and current exchange-correlation functionals lack the nonlocal contributions essential for the accurate modeling of a bond stretched to its breaking point, resulting typically in an underestimation of PT barrier heights. A further problem which arises in these simulations is the neglect of zero-point energy contributions (ZPC) in classical dynamics, which will result in an overestimation of the barrier height. There are therefore two competing deficiencies in our simulations, which will partially cancel in a fortuitous manner.³⁹ The pure DFT functional will underestimate the PT barrier, but the neglect of the ZPC will work against this to our favor.

In this work, we report on the structural stability of this model-system when subjected to ab initio MD calculations. The α -helix employed in this instance is the simplest possible, consisting of a right-handed helix of a single amino acid, glycine ($\text{NH}_2\text{CHRCOOH}$, where R = H, the side chain). We will demonstrate the importance of including dispersion interactions to stabilize the helical structure through the adoption of pair potential functions as suggested by Grimme.⁴⁰ We have studied

the effect of changing the density of water molecules contained within the cavity (comprising eight, ten, and twelve water molecules, respectively) and also studied the effect of introducing an extra proton to set up the water-wire system. Our simulations have allowed us to determine the nature and prevalence of various different cationic species that formed spontaneously during the MD simulations and to draw some conclusions regarding the mechanism of PT within a hydrated α -helical channel environment. It must of course be stressed that the structures of actual trans-membrane channels are significantly more complex than our model allows. Our work does however help to narrow the gap between the constrained environment models previously reported and the fully atomistic protein studies that can only be modeled using lower-level computational techniques.

II. Simulation Methods

A. Model. A polypeptide chain of glycine was twisted into a right-handed α -helix (with standard φ and ψ angles of -57.0° and -47.0° , respectively) using the ARGUSLAB⁴¹ polypeptide builder. The simulation was run under full periodic boundary conditions (PBCs) by placing one full repeat of the helix (i.e., four helical turns, comprising 15 amino acid residues) at the corner of an orthorhombic cell to lie along cell vector b , corresponding to 26.36 Å (see Figure 1). Thus, cell vector a ($= c$, initially set to 8.0 Å) defines the diameter of the interhelical pore, into which the water environment (comprising in turn eight, ten, and twelve water molecules, plus an extra proton) is placed. In this way, the one helix model is replicated to four, and in turn this packing arrangement is repeated to infinity along the a , b , and c vectors (see Figure 2). Note the total number of atoms for this model is less than 150, and so it is accessible to full quantum mechanical treatment.

B. Simulations. All simulations were run using the CP2K^{42,43} molecular dynamics simulation package with the GGA Becke–Lee–Yang–Parr (BLYP)^{44,45} functional, coupled to a dual localized (Gaussian) and plane-wave basis set description. The localized basis set was of double- ζ quality and optimized for use against the Goedecker–Teter–Hutter set of pseudopotentials⁴⁶ coupled to the BLYP functional. A series of single-point energy calculations determined the optimum energy cutoff (300 Ry), and the subsequent geometry optimization was performed in two steps using the Broyden–Fletcher–Goldfarb–Shanno (BFGS)^{47–50} method. In the first instance, atom positions only were allowed to relax; this was then followed by a series of single-point energy calculations to obtain the optimized cell vectors, during which the b vector shortened slightly (to 26.26 Å) while the a and c vectors remained unchanged. The water-wire model was then constructed by adding an extra hydrogen atom to one of the water molecules to create an oxonium ion, $[\text{H}_3\text{O}]^+$. The eight and twelve water-wire models were then built from this baseline model, by removing or adding two further water molecules, respectively. All three models were then subjected to atom minimization, which then formed the starting points for NVT ab initio molecular dynamics equilibration simulations. Dispersion, or van der Waals, interactions, which are inherently missing from DFT calculations, were accounted for by the addition of a pair potential.⁴⁰ The MD simulations (maintained at 365 K by a chain of Nose–Hoover thermostats) were run using the same basis set as described above for ca. 25 ps, advancing in time increment steps of 0.55 fs. After these equilibration runs, the production runs (of at least 25 ps) were then obtained under NVE conditions for each model. Visualization of the models and the MD trajectories was performed using the VMD package.⁵¹

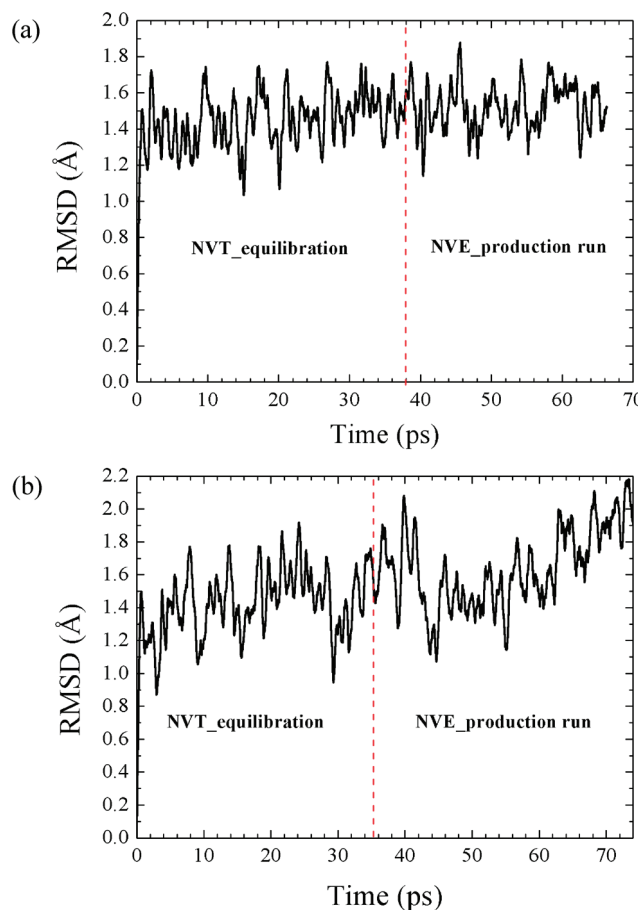


Figure 3. Relative mean square displacement (rmsd) of the helix backbone atoms for the ten water-wire model with (a) dispersion corrections included and (b) no dispersion correction.

III. Results and Discussion

A. Structural Stability of the Model. In this study, the model used is a single α -helix and water environment under PBCs with no atomic positional restraints, and thus the stability of the model must be checked. The integrity of the PBC along the b vector was tested by verifying that the time-average C–N bond (which forms the continuous helix by bridging the cell boundary) is consistent with the time-averaged C–N bonds present in the rest of the helix. We compared the boundary value with three other C–N bonds presented in other parts of the helix, and all were found to be identical to within one standard deviation. This establishes that the boundary conditions remained intact throughout the simulation, and the channel can be modeled as continuous.

Figure 3 shows the root-mean-square deviation (rmsd) of the helix backbone over the course of two trajectories for our baseline model (comprising ten water molecules and an extra proton), relative to the initial ($t = 0$, i.e., optimized) structure. The plots show the importance of including the dispersion correction to prevent the helix from unravelling. With the correction in place [Figure 3(a)], the atom positions are shown to fluctuate noticeably, with an average displacement of 1.4(2) Å (and a maximum of 1.9 Å). Although there is no recognized standard or upper limit for the rmsd, previous studies are comparable to this one, reporting rmsd's in the range 1–1.5 Å.³² Crucially, most of the deviation occurs within the first picosecond of the simulation, after which the plot levels off which indicates that the helix does not unfold during the course of the simulation. In the absence of the dispersion correction

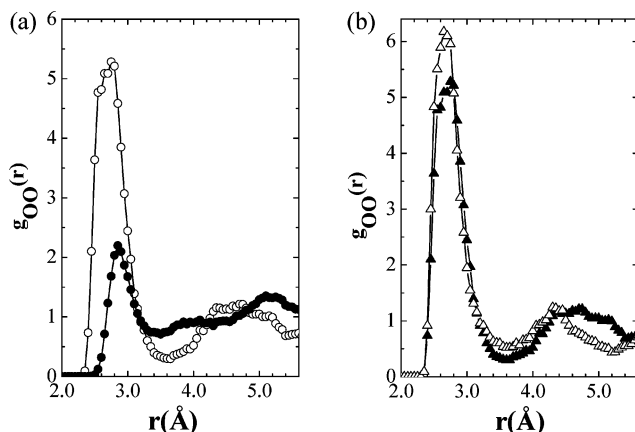


Figure 4. Radial distribution functions $g_{OO}(r)$ obtained from (a) the ten water molecule model (OO) (filled) and in the presence of an extra proton (O^*O) (open) using the BLYP functional and (b) similar plots obtained for the PBE functional.

[Figure 3(b)], a slightly higher average rmsd was obtained [1.5(3) Å with a maximum value of 2.2 Å]. However, this plot does not level off after the 25 ps equilibrium period, indicating likely breakdown of the helix in this case. Thus, we conclude that the dispersion interactions play a crucial role in stabilizing the α -helical structure, which echoes recent work on the DNA duplex.⁵²

The channel radius as a function of the b -axis was further investigated using the HOLE program,⁵³ which maps the internal cavity of the channel based on the maximum radii of a series of hard spheres. The resulting representation is given in Figure 2, where the radii of the hard spheres were observed to fluctuate around 2.1(2) Å for most of the channel. A minimum radius of 1.15 Å⁵⁴ is required to accommodate a water molecule, thus indicating that all parts of this channel are accessible to the water-wire.

B. Behavior of Water-Wire vs Water-Chain. The effect of introducing a proton to the chain of ten water molecules was investigated by a direct comparison of the oxygen–oxygen radial distribution functions (RDFs), $g_{OO}(r)$, obtained for the water-chain and water-wire systems. These plots, shown in Figure 4(a), provide information on the nature of the hydrogen bonding between the water molecules. Our results echo those of Voth et al. obtained from studying PT in cylindrical, smooth-walled hydrophobic channels.³² Considering first the $O\cdots O$ separations found for the water-wire, the dominant peak lies at 2.75 Å with density starting at 2.4 Å. Gas-phase calculations have shown an average donor–acceptor separation of around 2.4 Å for the Zundel complex, $[H_5O_2]^+$, and 2.57 Å for the Eigen complex³² (which is a central $[H_3O]^+$ ion solvated by three water molecules). On this basis we assign the shortest separations observed to the formation of the Zundel complex. Although we do see density at ca. 2.6 Å, we cannot attribute this to a standard Eigen complex as the channel width is too narrow to accommodate this type of solvation structure. We do, however, observe many instances of an Eigen-type structure with $O\cdots O$ separations of around this value, where the hydrogen bond of the third water in the bulk is replaced by a contact to a carbonyl oxygen of the helix backbone to form a “tethered” Eigen complex. Studies of excess protons in bulk water environments have suggested that of the two species the Eigen complex is the more stable.⁵⁵ Thus, it would appear that the formation of the tethered Eigen complex in our model channel represents an attempt to mimic this stable species.

The $O\cdots O$ separations observed on the RDF from the simulation without the excess proton show a general shift to longer separations (2.85 Å) between the water oxygen atoms, which is consistent with that reported on a $g(r)$ plot of bulk water.³¹ Comparison of the $g_{OO}(r)$ plots suggests that the effect of the excess proton extends beyond those water molecules immediately surrounding it and leads to a structuring of the water molecules in the next solvation shell, which is in agreement with previous findings.⁵⁶ This feature is absent on the water-chain plot, thus suggesting that in the absence of the extra proton the water molecules are considerably less organized and adopt a wider distribution, presumably due to the increased mobility of the less-coordinated channel water molecules.

C. Effect of Changing the Density of Water Molecules in the Channel. The simplified model employed in this work cannot support a water reservoir at either end of the interhelical pore. The simulation must therefore start with a predetermined number of water molecules already present in the pore, and so the effect of varying the density of water must be carefully checked. A comparison of the rmsd's for the eight, ten, and twelve water-wire models appears to suggest that altering the density of water molecules in the central cavity does influence the behavior of the helical scaffold. As the number of water molecules in the cavity is increased the average rmsd increases from 1.4 to 1.7 Å. This is perhaps not too surprising: the helix is over 26 Å long, and interactions with water molecules could easily activate low-energy transverse oscillations that are picked up in the rmsd plots.

Time-averaged plots obtained over 25 ps NVE trajectories for the eight, ten, and twelve water-wire models are given in Figure 5. Concentrating first on the ten-membered water-wire [Figure 5(b)], it is apparent that for the majority of the simulation at least five of the water molecules hydrogen bond to carbonyl groups on the α -helices. The excess proton travels over five (though predominantly four) of the ten water molecules, covering a distance of approximately 7.5 Å, or a quarter of the channel length, without any significant diffusion of the water molecules themselves. The pattern of hydrogen bonding within the wire and around the excess proton is seen to radiate from a central solvated oxonium ion, with the central water molecules participating in three hydrogen bonds (two with neighboring water molecules with a third contribution from a backbone carbonyl oxygen) and the outer in two (due to the loss of one hydrogen bond with a water molecule). The ordering of water molecules within the water-wire was further investigated using the average atomic distributions of water O- and H-atoms along the polyglycine channel axis, as shown in Figure 6. The plot has two distinct regions, with those water molecules involved in PT easily distinguished from those which are not. Strong hydrogen bonding within the wire is indicated by hydrogen atom peaks that are placed between successive oxygen atoms to form a regular donor–acceptor pattern [particularly so for oxygen atoms 6–9, see Figure 6(b)]. These four peaks show the preferred position of the excess proton, which is found in a conformation spread over four oxygen atoms. The donor–acceptor pattern radiates out from this central area, holding these four water molecules in a tight configuration, as indicated by the sharpness of the oxygen peaks. There is no diffusion here, but simply fluctuation around a set position. Five of the remaining water molecules (2–5, 10) are seen to form a water-chain separate from the water-wire, with the wider peaks indicating these water molecules have an increased mobility compared to those in the water-wire.

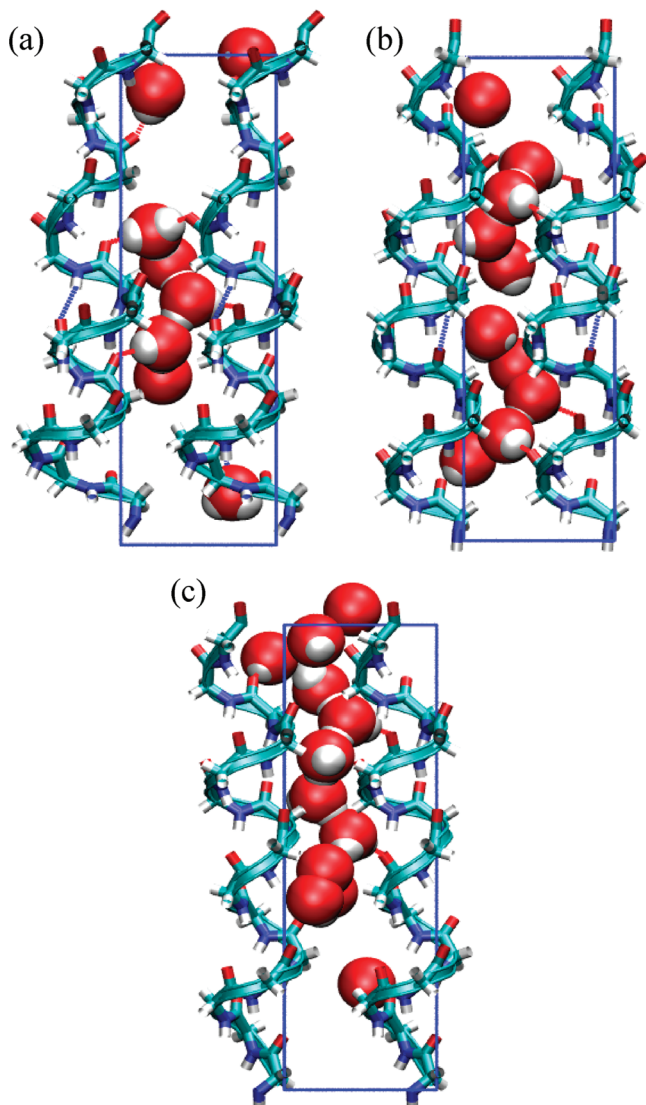


Figure 5. Time-averaged plots of the (a) eight-, (b) ten-, and (c) twelve-water-wire models. Note the water molecule numbering scheme used in the text is defined with respect to the bottom of each of these simulation cells.

A reduction in the number of water molecules in the wire has a very noticeable effect on its structure and dynamics [see Figures 5(a) and 6(a)]. The three central peaks of the O- and H-atom distributions again show the preferred position of the excess proton, which in this case is delocalized over two water molecules and a carbonyl oxygen on the α -helix to form an Eigen-type cation. Again, the donor–acceptor pattern radiates from the center, but in this case the order extends only to the central five water molecules. The rest are relatively mobile. The removal of two water molecules has therefore resulted in a further break in the water-wire, rendering a substantial volume of the channel dry. Proton transport cannot bridge this gap, which limits the distance the proton can travel to only 3.5 Å.

Adding two water molecules to the baseline ten-water-wire model also alters the behavior of the system significantly: the proton is now delocalized over six to seven water molecules and travels a distance of 10.5 Å [See Figures 5(c) and 6(c)]. The time-averaged structure, however, shows reduced hydrogen bonding between the water-wire and the helix carbonyl groups with only three water molecules shown to participate in bonding. The O- and H-atom distributions show five or six water molecules held strongly around the excess proton, while those

beyond this sphere of influence are considerably more mobile, particularly water molecules 3–5. The time-averaged structure [Figure 5(c)] shows a small break in the water-wire between molecules 1 and 2 and 2 and 3. The O- and H-atom distributions, however, do not show this same feature but do indicate a greatly increased mobility, which when averaged out may result in this artifact.

The average lifetimes of the different cationic states (i.e., $[H_{2n+1}O_n]^+$, where $n = 2–10$) that were created during the MD trajectories can be obtained by defining a time autocorrelation function for bond existence as

$$C_e(t) = \frac{1}{N} \sum_{i=1}^N \langle \alpha(0) \times \alpha(t) \rangle$$

where $\alpha(t)$ is defined to be 1 if the interaction condition between a pair of atoms is met at time t and 0 if it is not. A hydrogen bond was defined by considering interactions between oxygen atoms that fell within a cutoff distance of $R_{OO} \leq 3.5$ Å, which was chosen to encapsulate the first peak on the $g_{OO}(r)$ plot shown in Figure 3(a), along with an H–O…O angle constraint of 30°. The first step in the process is to identify the oxygen atom which has the three closest hydrogen atoms, i.e., the oxonium ion (denoted O^*). From there, to track a Zundel cation $[H_5O_2]^+$ the O…O distance from O^* to a neighboring water molecule must be less than or equal to 2.75 Å, and these in turn must be separated from all other water molecules by a distance greater than 3.5 Å. Extensions to this methodology then allow for the higher hydrated cation species (i.e., the proton delocalized over three, four, or five water molecules) to be similarly investigated. Integration of the resulting time autocorrelation functions then yields the corresponding cation lifetimes. In addition, the production run MD trajectories were analyzed to count the number of instances that the geometric criteria for the existence of the individual cationic states were fulfilled. The results, along with the lifetimes, are given in Table 1. From this, we see that there is a wide range in cationic state lifetimes, from tens of femtoseconds to several picoseconds. We also observe that there is a rough correlation between the lifetimes and the prevalences for each state; i.e., in general, the more times the state is formed, the longer its lifetime. At no point was an isolated Zundel ($n = 2$) cation observed; however, the $n > 3$ states may contain the Zundel structure solvated by $n - 2$ water molecules. All results are consistent with the time-averaged plots in Figure 5 and the average water distributions in Figure 6.

The baseline ten-water-wire model supports the formation of water-wires from $n = 2$ to 9 but shows a clear preference for the four-membered water-wire state (i.e., $[H_9O_4]^+$). This state has a very long lifetime of 2.6 ps, reinforcing this as the most stable cationic state for the ten-water-wire model. The reason for this lies with the fact that the water-wire in this model broke halfway through the simulation, after which time the simulation essentially settled into the $[H_9O_4]^+$ state. The observation of states $n = 7–9$ with lifetimes of several hundreds of femtoseconds relate to the first half of the simulation before the wire broke. Intermediate states of $n = 5–6$ were also observed but with very short lifetimes that correspond to the time scale of the O–H bond stretching vibration.

The eight-water-wire model distribution peaks at $n = 5$, the creation of which was observed for over 95% of the simulation. Wires above five water molecules in length are not observed in the trajectory, as the loss of two water molecules creates two breaks in the overall water-wire and the excess proton is

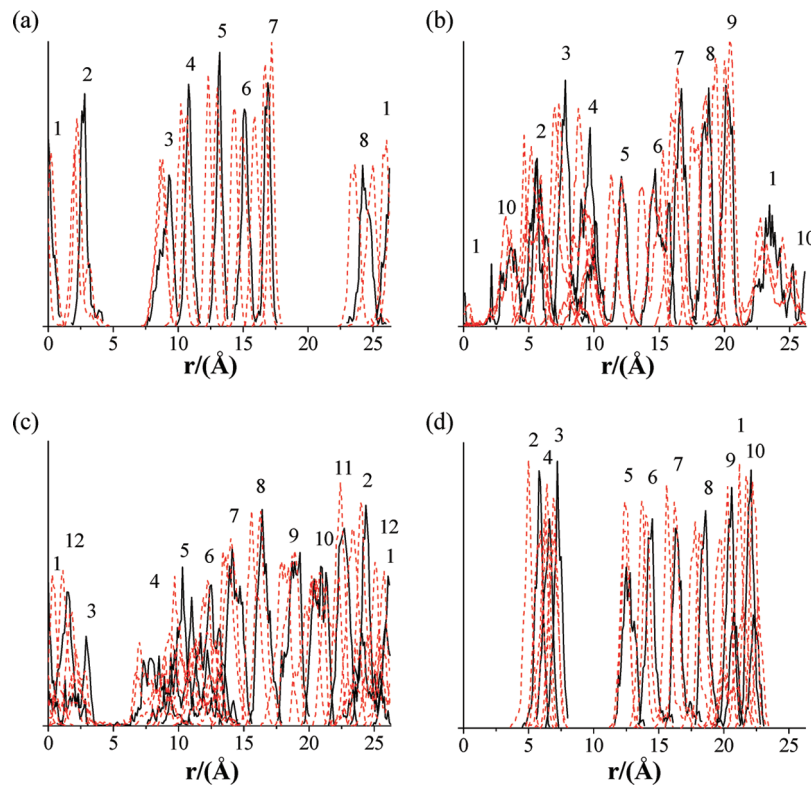


Figure 6. Average atomic distributions of water oxygen (black solid line) and hydrogen (red dashed line) atoms modeled along the channel axis for the (a) eight-, (b) ten-, and (c) twelve-water-wire models. Also shown is the (d) ten-water-wire model system using the PBE functional.

TABLE 1: Prevalences (Expressed as a % of the Total Simulation Time) and Lifetimes (in fs) of the Cationic States $[\text{H}_{2n+1}\text{O}_n]^+$ Observed in the Eight-, Ten-, and Twelve-Water-Wire Models

<i>n</i>	8-water-wire		10-water-wire		12-water-wire	
	prevalence	lifetime	prevalence	lifetime	prevalence	lifetime
3	2.4	32	0.5	9	0.01	4
4	1.4	10	43.7	2569	0.7	64
5	96.2	19	4.7	53	3.6	151
6	-	-	2.2	22	31.3	964
7	-	-	12.3	942	17.4	489
8	-	-	18.6	210	6.2	196
9	-	-	18	517	13.2	400
10	-	-	0.1	10	27.9	774

confined to the central region of the channel [Figure 6(a)]. The lifetimes for this model indicate that the system is extremely fluxional, with all species decaying on the femtosecond time scale. Finally, the twelve-water model shows a preference for the formation of longer water-wires, peaking at $n = 6$ and $n = 10$.

D. Mechanism for PT in a Model α -Helical Channel. Recent work on bulk water simulations^{57,58} has made use of $g_{\text{OH}}(r)$ RDFs centered on the oxonium oxygen (O^*), the oxygen which will accept the proton (O_{next}), and its other nearest neighbors ($\text{O}_{\text{nearest}}$) averaged over the whole simulation to try to elucidate a mechanism for the PT process. A successful PT event is defined as one where the next transfer event does not see the proton simply reverse its direction. These reversals are unsuccessful and are termed “rattling” events. For direct comparison with this work, we present our data for the ten-water-wire model in this format. Figure 7 shows a series of time-dependent $g_{\text{OH}}(r)$ RDFs centered on O_{next} and $\text{O}_{\text{nearest}}$ at four time intervals leading up to a PT step: (a) well before the event and (b)–(d) the time directly preceding it. An average is taken over all PT steps, with the rattling events excluded.

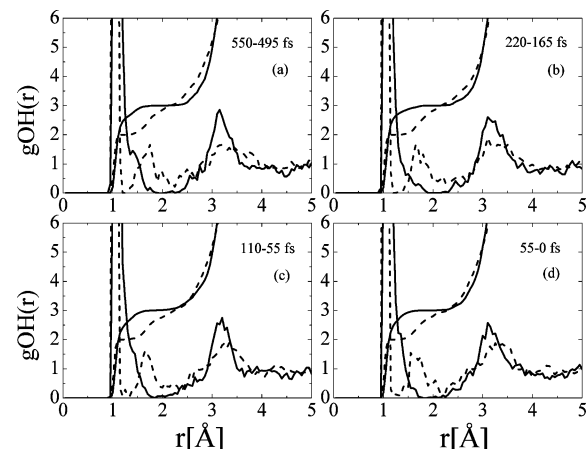


Figure 7. Time-dependent RDFs and integrated coordination number plots of O_{next} (solid black line) and $\text{O}_{\text{nearest}}$ (dashed black line) averaged over 55 fs intervals before [(a) 550–495 fs] and approaching a PT event [(b) 220–165 fs, (c) 110–55 fs, and (d) 55–0 fs]. PT occurs at time 0 in panel (d).

For ease of discussion, we consider first the $\text{O}_{\text{nearest}} g(r)$ plot (dashed black line, Figure 7). The dominant, sharp peak is centered at 1.1 Å, which can be assigned to the hydrogen atoms directly bound to the oxygen atoms to form a water molecule. A second, broader peak is centered at around 1.7 Å, which corresponds to an $\text{O} \cdots \text{H}$ hydrogen bond interaction and a third broader peak at around 3.3 Å which is an $\text{O} \cdots \text{H}$ distance over a wider coordination sphere. This plot remains essentially constant throughout the four time intervals, indicating that the $\text{H}_2\text{O}_{\text{nearest}}$ molecule does not play a role in the PT mechanism. The $\text{O}_{\text{next}} g(r)$ plot (solid black line, Figure 7) does, however, show important changes over the time intervals shown. The three peaks are again present: the dominant peak at 1.1 Å, the second peak which now appears as a shoulder at ca. 1.4 Å, and the

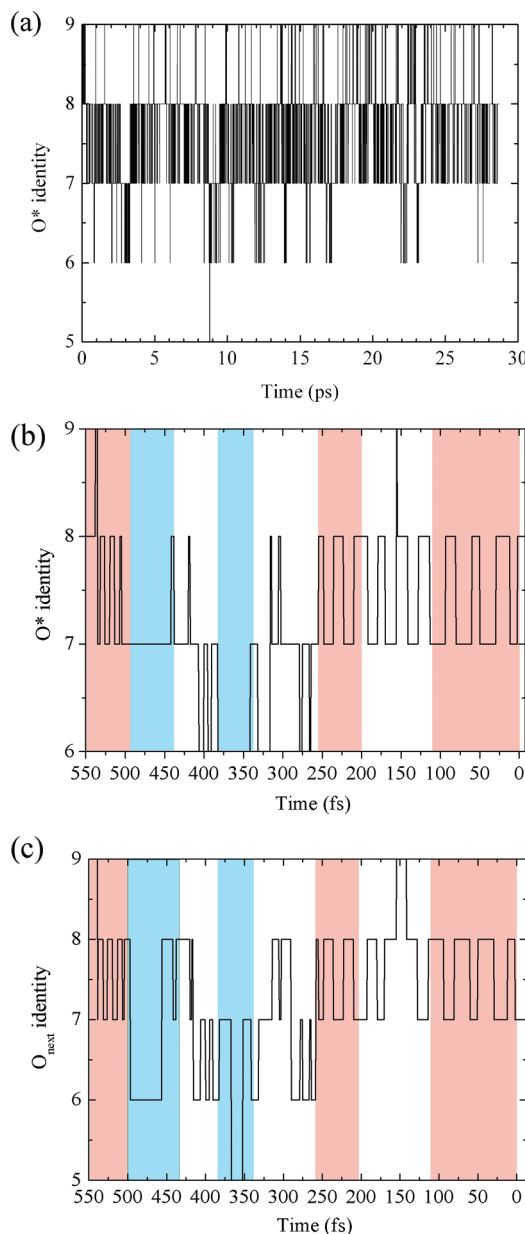


Figure 8. Plot of oxonium identity vs time for (a) the whole MD production run, (b) the time interval leading up to a PT event, and (c) the identity of O_{next} over the same time interval. The pink shaded panels correspond to the time intervals given in Figure 7(a)–(d) and the blue to regions where the identity of O^* remains fixed for short periods of time.

third peak which is now sharper and centered around a slightly shorter distance of ca. 3.1 Å. The fact that the second peak appears at a shorter distance makes perfect sense: the $[\text{H}_3\text{O}]^+$ and $\text{H}_2\text{O}_{\text{next}}$ molecules are closer together, hence the heightened incidences of PT rattling events. During the time period leading up to the PT event, this peak shifts to the left (from 1.4 to 1.3 Å) demonstrating the formation of the short, strong hydrogen bond indicative of a Zundel cation, $[\text{H}_2\text{O}_5]^+$. This peak shift agrees with previous findings,⁵⁸ but we acknowledge that our data are less clear, as our second peak appears as a shoulder rather than a distinct second peak.

In our channel model, all successful PT steps are preceded by a large number of unsuccessful or rattling PT events as described above. This is shown in Figure 8(a), where the identity of the oxonium ion versus time for the whole of the MD production run is displayed in the same manner as Markovitch

et al. for bulk water.⁵⁷ The rattling events are evident from the large number of incidences where the O^* identity repeatedly flips with a neighbor (O_{next}). A plot leading up to one particular PT event that highlights the representative time intervals presented in Figure 7 is shown in Figure 8(b), where the constant fluctuations prior to the PT event can be clearly seen. The large number of rattling events can be traced back to the fact that the direction of PT is limited in the channel environment and the positions of the water molecules are inevitably constrained by the presence of the helix. To continue the comparison with bulk water, we also track the identity of O_{next} [shown in Figure 8(c)] over the same time interval shown in Figure 8(b). In bulk water, the excess proton resides on one particular water molecule for sustained periods of time, which allows for detailed analysis of the corresponding behavior for $O_{\text{next}}/O_{\text{nearest}}$. During these stable periods, it is possible to see fluctuations in O_{next} identity, such that the three water molecules in the first solvation shell compete to get closest to O^* . This has been termed the “special pair dance”.⁵⁷ In our channel environment, the heightened incidences of rattling mean we do not observe the same long periods of time where the identity of O^* remains fixed. During the short time periods [Figure 8(b)] where O^* does not change, there is some evidence of O_{next} flipping [Figure 8(c)]. However, the statistical certainty is lacking to state conclusively whether the special pair dance phenomenon found in bulk water also exists in the channel simulations.

One further significant deviation from the bulk water mechanism of PT can be identified. In bulk water simulations, a key step to successful PT is the Eigen–Zundel–Eigen isomerizations (E–Z–E)^{36,59} which indicate the importance of hydrogen bond cleavage to successful PT. The previous work⁵⁸ validated this E–Z–E theory as analysis of the oxygen atom coordination number clearly showed the breaking and formation of hydrogen bonds along the PT trajectory: O_{next} loses a hydrogen bond (the coordination drops from four to three), and O^* gains a hydrogen bond (the coordination rises from three to four). A channel environment cannot support the same characteristics, as it imposes natural limits on the number of hydrogen bonds a water molecule can form. In our simulation, a maximum value of three is observed (see Figure 7); i.e., two hydrogen atoms are directly coordinated to the oxygen atom, and a third is accepted from a neighboring water molecule. Thus we can conclude that the water molecules in the channel are coordinatively unsaturated. In the case of the close hydrogen bonded network involved in PT, this coordination number will not change; i.e., unlike bulk water, the breaking of a hydrogen bond is not a precursor to a successful transfer event. This study therefore highlights an important difference in the PT mechanism for a channel environment compared to bulk water.

Finally, as our model is more chemically relevant than the work that has gone before us,^{29–34} we should be able to report more on the properties specific to an α -helical channel environment. We observed some evidence from rmsd plots that as the density of water in the channel increases the amount of helical movement also increases. Looking more closely at the time-averaged pictures in Figure 6 also suggests that the active PT regions of the water-wire correspond with those areas of the helix that are most tightly coiled. Or conversely, water diffusion behavior is observed over those regions where the helix has undergone the most visible change. This is particularly noticeable in the top section of the eight-water-wire model [Figure 5(a)] and the bottom section of the twelve-water-wire model [Figure 5(c)]. This would suggest that when there is a clearly defined helical groove the water molecules will adopt favorable

positions that are capable of displaying longer-range cooperative behavior and thus can support PT.

E. Effect of Changing the DFT Functional on the Behavior of the Water-Wire. It is well-known that current GGA functionals do not accurately describe the behavior and properties of water molecules in the bulk, with, e.g., diffusion rates and hydrogen bond donor–acceptor distances not correctly represented during the MD simulation,⁶⁰ although recent evidence would suggest that the use of a complete basis set greatly improves the properties mentioned above.⁶¹ There is however little documentation on the effects of different functionals on the properties of water molecules within a water-wire. To address this point further, MD simulations on the baseline ten water molecule model with and without an extra proton were carried out using the PBE functional as expressed in the CP2K package, with all other conditions consistent with the BLYP baseline model reported above. Analysis of the trajectories revealed that there are significant differences in the behavior of the wire with the choice of functional.

Comparison of the $g_{OO}(r)$ plots of the ten-water-wire baseline model MD simulations using BLYP and PBE functionals shows a distinct difference in the structuring and behavior of the water-wire [compare Figure 4(a) with 4(b)]. The PBE plot shows a shift to shorter OO separations, with the distribution peaking at 2.65 Å compared to the 2.75 Å maximum for the BLYP model, which is itself in good agreement with experiment.⁶² The secondary solvation shell is much more distinct in the PBE wire-model with a narrower, more defined peak at 4.3 Å as opposed to the larger spread observed for the BLYP model.

The O- and H-atom distribution plots for the two functionals again illustrate the effects of varying the functional on the formation and dynamics of the proton wire [compare Figure 6(b) and 6(d)]. The PBE model demonstrates an increased structuring of the water molecules, with all but one water molecule held in a tight conformation. The influence of the excess proton is increased to six water molecules, but those molecules that have broken off from the main water-wire are themselves held in an extremely tight hydrogen-bonding pattern, as shown by the narrow, sharp distribution.

We also note that from a structural chemistry perspective the orientations of the water molecules within the wire in the PBE model are in more optimal positions for PT than observed in the BLYP simulation, and yet the overall degree of PT observed with this functional is suppressed. While the proton does travel over six of the water molecules, around 96% of its time is spent on O(9) and O(8). There are therefore significantly fewer successful PT events and greatly increased unsuccessful rattling events. From these results, we therefore conclude that the BLYP functional appears to provide a more dynamical description of the water-wire. Previous work⁶³ tested the accuracy of common density functional methods using six- and eight-water clusters. Using MP2 calculations as a benchmark, they found that while the PBE functional provided a closer estimate of the geometry the BLYP functional calculated the energy to a greater level of accuracy. Overall, the hybrid functional B3LYP was suggested as the best DFT functional for this purpose. However, from an ab initio molecular dynamics perspective we note that any higher level functional that makes use of the Fock matrix for exact exchange is likely to remain intractable when coupled to a plane-wave basis set for some time to come.

IV. Conclusions

A very simple model for a trans-membrane protein channel that supports PT has been successfully constructed and subjected

to various ab initio MD simulations. The maximum distance traveled for an excess proton along a chain of water molecules in the absence of any external driving force is approximately 10.5 Å, which corresponds to around 1.5 helical turns. The addition of an excess proton to a water chain was observed to set up long-range cooperativity between water molecules, with evidence of the formation of second solvation shells observed in $g(r)$ plots. This is consistent with previous findings. The effect of altering the number of water molecules within the channel was also investigated. Some evidence was observed that the water molecules exerted some influence on the behavior of the helix, with the rmsd for the model increasing slightly with water density. It was also observed that the regions of the channel that supported PT, rather than water diffusion, were those that were more tightly coiled. Within the wire, a range of cationic species were observed, with lifetimes recorded over a wide range (from 10 fs to 2.6 ps).

The mechanism for PT in this α -helix channel model showed significant differences from that observed for bulk water. The Eigen–Zundel–Eigen isomerizations necessary for the propagation of an excess proton through bulk water are not possible in the channel environment. We observe that the number of coordinated hydrogen atoms around an oxygen atom remains constant at three; i.e., it is not necessary to break a hydrogen bond for PT to occur as has been reported in bulk water simulations. Instead, there is a heightened incidence of proton “rattling” events throughout the simulation, where the proton constantly flips between two neighboring molecules. Consequently, the amount of time the excess proton stays coordinated to any one particular water molecule is reduced, and the statistical certainty to state whether or not the bulk-water “special pair dance” phenomenon occurs in the channel environment could not be obtained. In common with the bulk water mechanism, however, in the lead up to PT, we do observe a shortening of the O* to O_{next} hydrogen bond distance indicative of the formation of a Zundel complex.

Finally, we comment on the use of different computational models for an α -helix water-wire system. Our results suggest that the PBE functional overstructures the water-wire and suppresses PT while the DFT functional BLYP provides a more dynamical water-wire system. Our results also demonstrate the importance of including dispersion interactions in DFT simulations containing α -helical structures.

Acknowledgment. C.A.M. acknowledges the Royal Society for the award of a University Research Fellowship, and L.M.S.S. an EaSTCHEM scholarship. This work is supported by the EPSRC under grant EP/G040656/1 and has made use of the resources provided by the EaSTCHEM Research Computing Facility (<http://www.eastchem.ac.uk/rcf>). This facility is partially supported by the eDIKT initiative (<http://www.edikt.org>). This work also made use of the facilities of HPCx, the UK’s national high-performance computing service, which is provided by EPCC at the University of Edinburgh and by STFC Daresbury Laboratory and funded by the Department for Innovation, Universities and Skills through EPSRC’s High End Computing Programme.

References and Notes

- (1) Swanson, J. M. J.; Maupin, C. M.; Chen, H.; Petersen, M. K.; Xu, J.; Wu, Y.; Voth, G. A. *J. Phys. Chem. B* **2007**, *111*, 4300–4314.
- (2) Decoursey, T. E. *Physiol. Rev.* **2003**, *83*, 475–579.
- (3) Wright, C. A. *Biochim. Biophys. Acta, Bioenergetics* **2006**, *1757*, 886–912.
- (4) Subramaniam, S.; Hirai, T.; Henderson, R. *Philos. Trans. R. Soc. A* **2002**, *360*, 859–874.

- (5) Nishimura, K.; Kim, S.; Zhang, L.; Cross, T. A. *Biochemistry* **2002**, *41*, 13170–13177.
- (6) Braun, T. F.; Al-Mawsawi, L. Q.; Kojima, S.; Blair, D. F. *Biochemistry* **2004**, *43*, 35–45.
- (7) Preston, G. M.; Carroll, T. P.; Guggino, W. B.; Agre, P. *Science* **1992**, *256*, 385–387.
- (8) Findlay, J.; Eliopoulos, E. *Trends Pharmacol. Sci.* **1990**, *11*, 492–499.
- (9) Pardo, L. J.; Ballesteros, J. A.; Osman, R.; Weinstein, H. *Proc. Natl. Acad. Sci. U.S.A.* **1992**, *89*, 4009–4012.
- (10) Patny, A.; Desai, P. V.; Avery, M. *Curr. Med. Chem.* **2006**, *13*, 1667–1691.
- (11) Luecke, H.; Schobert, B.; Richter, H.-T.; Cartailler, J.-P.; Lanyi, J. K. *J. Mol. Biol.* **1999**, *291*, 899–911.
- (12) Schmitt, U. W.; Voth, G. A. *J. Phys. Chem. B* **1998**, *102*, 5547–5551.
- (13) Day, T. J. F.; Soudackov, A. V.; Cuma, M.; Schmitt, U. W.; Voth, G. A. *J. Chem. Phys.* **2002**, *117*, 5839–5849.
- (14) Wu, Y.; Chen, H.; Wang, F.; Paesani, F.; Voth, G. A. *J. Phys. Chem. B* **2008**, *112*, 467.
- (15) Riccardi, D.; Schaefer, P.; Yang, Yu, H.; Ghosh, N.; Prat-Resina, X.; Konig, P.; Li, G.; Xu, D.; Guo, H.; Elstner, M.; Cui, Q. *J. Phys. Chem. B* **2006**, *110*, 6458–6469.
- (16) Ignacio Fdez, G.; Anne, V.; Juan, C. F.-C.; Martin, J. F. *Proteins* **2008**, *73*, 195–203.
- (17) Kandt, C.; Gewert, K.; Schlitter, J. *Proteins* **2005**, *58*, 528–537.
- (18) Rousseau, R. V. K.; Kleinschmidt, V.; Schmitt, U. W.; Marx, D. *Angew. Chem., Int. Ed.* **2004**, *43*, 4804–4807.
- (19) Lee, Y.-S.; Krauss, M. *J. Mol. Struct.* **2004**, *700*, 243–246.
- (20) Smolyanov, A. M.; Voth, G. A. *Biophys. J.* **2002**, *83*, 1987–1996.
- (21) Chen, H.; Wu, Y.; Voth, G. A. *Biophys. J.* **2007**, *93*, 3470–3479.
- (22) Xu, J.; Sharpe, M. A.; Qin, L.; Ferguson-Miller, S.; Voth, G. A. *J. Am. Chem. Soc.* **2007**, *129*, 2910–2913.
- (23) Cukier, R. I. *Biochim. Biophys. Acta, Bioenergetics* **2004**, *1656*, 189–202.
- (24) Wikström, M.; Verkhovsky, M. I.; Hummer, G. *Biochim. Biophys. Acta, Bioenergetics* **2003**, *1604*, 61–65.
- (25) Zheng, X.; Medvedev, D. M.; Swanson, J.; Stuchebrukhov, A. A. *Biochim. Biophys. Acta, Bioenergetics* **2003**, *1557*, 99–107.
- (26) Lear, J. D.; Wasserman, Z. R.; DeGrado, W. F. *Science* **1988**, *240*, 1177–1181.
- (27) Wu, Y.; Ilan, B.; Voth, G. A. *Biophys. J.* **2007**, *92*, 61–69.
- (28) Wu, Y.; Voth, G. A. *Biophys. J.* **2003**, *85*, 864–875.
- (29) Chen, H.; Ilan, B.; Wu, Y.; Zhu, F.; Schulter, K.; Voth, G. A. *Biophys. J.* **2007**, *92*, 46–60.
- (30) Pomes, R.; Roux, B. *J. Phys. Chem.* **1996**, *100*, 2519–2527.
- (31) Pomes, R.; Roux, B. *Biophys. J.* **1998**, *75*, 33–40.
- (32) Brewer, M. L.; Schmitt, U. W.; Voth, G. A. *Biophys. J.* **2001**, *80*, 1691–1702.
- (33) Dellago, C.; Hummer, G. *Phys. Rev. Lett.* **2006**, *97*, 245901, 1–4.
- (34) Dellago, C.; Naor, M. M.; Hummer, G. *Phys. Rev. Lett.* **2003**, *90*, 105902, 1–4.
- (35) Hummer, G. *Mol. Phys.* **2007**, *105*, 201–207.
- (36) Agmon, N. *Chem. Phys. Lett.* **1995**, *244*, 456–462.
- (37) Sagnella, D. E.; Laasonen, K.; Klein, M. L. *Biophys. J.* **1996**, *71*, 1172–1178.
- (38) Branden, C.; Tooze, J. *Introduction to Protein Structure*, 2nd ed.; Garland Publishing, Inc.: New York, 1999.
- (39) Durlak, P.; Morrison, C. A.; Middlemiss, D. S.; Latajka, Z. *J. Chem. Phys.* **2007**, *127*, 064304–8.
- (40) Grimme, S. *J. Comput. Chem.* **2006**, *27*, 1787–1799.
- (41) Thompson, M. A. *ArgusLab 4.0.1*; Planaria Software LLC: Seattle, WA.
- (42) The CP2K developer's group, 2008, <http://cp2k.berlios.de>.
- (43) VandeVondele, J.; Krack, M.; Mohamed, F.; Parrinello, M.; Chassaing, T.; Hutter, J. *Comput. Phys. Commun.* **2005**, *167*, 103–128.
- (44) Becke, A. D. *Phys. Rev. A* **1988**, *38*, 3098.
- (45) Lee, C.; Yang, W.; Parr, R. G. *Phys. Rev. B* **1988**, *37*, 785.
- (46) Hartwigsen, C.; Goedecker, S.; Hutter, J. *Phys. Rev. B* **1998**, *58*, 3641–3662.
- (47) Broyden, C. G. *J. I. Math. Appl.* **1970**, *6*, 222–231.
- (48) Fletcher, R. *Comput. J.* **1970**, *13*, 317–322.
- (49) Goldfarb, D. *Math. Comput.* **1970**, *24*, 23–36.
- (50) Shanno, D. F. *Math. Comput.* **1970**, *24*, 647–656.
- (51) Humphrey, W.; Dalke, A.; Schulter, K. *J. Mol. Graphics* **1996**, *14*, 33–38.
- (52) Rezac, J.; Pavel, H. *Chem.—Eur. J.* **2007**, *13*, 2983–2989.
- (53) Smart, O. S.; Neduvvelil, J. G.; Wang, X.; Wallace, B. A.; Sansom, M. S. P. *J. Mol. Graphics* **1996**, *14*, 354–360.
- (54) Smart, O. S.; Goodfellow, J. M.; Wallace, B. A. *Biophys. J.* **1993**, *65*, 2455–2460.
- (55) Schmitt, U. W.; Voth, G. A. *J. Chem. Phys.* **1999**, *111*, 9361–9381.
- (56) Markovitch, O.; Agmon, N. *J. Phys. Chem. A* **2007**, *111*, 2253–2256.
- (57) Markovitch, O.; Chen, H.; Izvekov, S.; Paesani, F.; Voth, G. A.; Agmon, N. *J. Phys. Chem. B* **2008**, *112*, 9456–9466.
- (58) Berkelbach, T. C.; Lee, H.-S.; Tuckerman, M. E. *Phys. Rev. Lett.* **2009**, *103*, 238302.
- (59) Lapid, H.; Agmon, N.; Peterson, M. K.; Voth, G. A. *J. Chem. Phys.* **2005**, *122*, 014506, 1–11.
- (60) VandeVondele, J.; Mohamed, F.; Krack, M.; Hutter, J.; Sprik, M.; Parrinello, M. *J. Chem. Phys.* **2005**, *122*, 014515–6.
- (61) Lee, H.-S.; Tuckerman, M. E. *J. Chem. Phys.* **2006**, *125*, 154507–14.
- (62) Hura, G.; Sorenson, J. M.; Glaeser, R. M.; Head-Gordon, T. *J. Chem. Phys.* **2000**, *113*, 9140–9148.
- (63) Svozil, D.; Jugwirth, P. *J. Phys. Chem. A* **2006**, *110*, 9194.

JP910262D